STUDY OF THE EFFECT OF SOIL SEEPAGE ON BURIED PIPE HEAT TRANSFER BASED ON LBM

Rui Wu[1], Shunyu Su[2], Nanxing Li[3]

[1]School of Urban Construction, Wuhan University of Science and Technology
(Qingling Street, Hongshan District, Wuhan 430070, Hubei Province, China)
E-mail: 2531631342@qq.com
[2]Professor, School of Urban Construction, Wuhan University of Science and Technology
(Qingling Street, Hongshan District, Wuhan 430070, Hubei Province, China)
E-mail: shunyusu@qq.com
[3] School of Urban Construction, Wuhan University of Science and Technology
(Qingling Street, Hongshan District, Wuhan 430070, Hubei Province, China)
E-mail: 1018581794@qq.com

In this paper, the quartet structure generation set (QSGS) was used to establish a wet saturated soil model which is similar to the real soil internal structure. And using the lattice Boltzmann method (LBM), the two-dimension case of groundwater seepage with the same depth of equivalent temperature distribution of the soil around equivalent buried pipe was simulated. The influences of porosity, seepage velocity, soil looseness, thermal conductivity of soil skeleton and thermal conductivity of backfill material on temperature distribution were studied. The simulation results show that with the increase of porosity and seepage velocity, the existence of seepage can effectively reduce the average soil temperature, and the effect of seepage can be almost ignored when the solid thermal conductivity is higher than 5.5 W/ (m·K). Meanwhile, the average soil temperature and the degree of soil looseness have irregular changes.

Key Words: *Quartet Structure Generation Set, Lattice Boltzmann Method, groundwater seepage, temperature distribution*

1. INTRODUCTION

As an air conditioning technology that utilizes shallow geothermal energy to achieve regional cooling and heating, ground source heat pump (GSHP) plays a significant role in reducing the use of fossil energy and protecting the environment, and it has been highly valued by many countries in the world. The vertical buried pipe ground source heat pump is widely used as one of the forms of ground source heat pump. The working efficiency of the ground source heat pump system largely depends on the heat exchange between the buried pipe heat exchanger and the soil. Studies have pointed out that the thermal physical properties of the soil and the heat transfer process of groundwater seepage of ground heat exchanger can produce certain effect[1- 5], but the soil as a typical porous medium, physics properties greatly depends on the microstructure of the soil, so the flow and heat transfer in the treatment of the related problems are

very important while there are two difficulties: on the one hand, it is difficult to get close to the real internal structure of soil; on the other hand, the internal structure of porous media is complex, and the boundary conditions of traditional CFD method are complex and programming is difficult.

Wang et al.[6] proposed the Quartet Structure Generation Set (QSGS) method, and obtained the Structure of porous media close to the real through computer simulation[7-9], thus solving the problem of modeling of porous media. Lattice Boltzmann Method (LBM) has attracted much attention in recent decades. Compared with traditional methods, the Lattice Boltzmann Method has advantages such as good parallelism, easy boundary processing and clear physical meaning. It is often used to deal with multiphase flow, seepage and heat transfer in porous media, chemical reaction flow and other fields where traditional methods are limited in research. Shao Baoli et al.[10] used LBM to conduct three-dimensional simulation of fluid flow in porous media, and analyzed the seepage law of fluid flow in Darcy zone, weak inertia zone and Forchheimer zone in porous media. The simulation results were compared with the basic seepage formula, which was in good agreement. Gao et al.[11] proposed a modified lattice Boltzmann model for conjugate heat transfer in systems considering both porous and other media. It has been verified that this model can be used as a feasible tool for studying conjugate heat transfer in porous media. Xu et al.[12] proposed a lattice Boltzmann model for infiltration of unfrozen water in saturated soil in the freezing process. By simulating the unfrozen water content and water conductivity of sandy soil and silty loam soil, and comparing the results with the experimental results, the two are in good agreement, indicating that the model is reliable.

In this paper, first using the method of QSGS structure model of two-dimensional ground heat exchanger, and then through the establishment of incompressible coupling double distribution function based on Boussinesq hypothesis lattice Boltzmann model(DDF-LBM), simulation of different seepage velocity, porosity, soil particle size distribution, soil coefficient of thermal conductivity of circumstances such as ground heat exchanger heat transfer situation, analysis the soil internal pore water seepage velocity, and the change trend of soil temperature. By comparing and analyzing the heat transfer situation with that in the case of no seepage, the heat transfer law of buried pipe heat exchanger in the case of seepage is revealed. It would provide theoretical guidance for the optimization of the design of buried pipe ground source heat pump.

All the simulation calculations in this study are programmed by MATLAB software.

2. LBM THEORYANDVERIFICATION

(1) LBM model

This paper uses the incompressible coupled lattice Boltzmann model with double distribution function based on Boussinesq hypothesis, which was first proposed by Guo et al[13] in 2002. The model contains two distribution functions of velocity and temperature. The coupling of temperature field and velocity field is realized by adding an external force term to the right of the equal sign of velocity distribution function. In this study, the D2Q9 model is used to simulate the velocity field and temperature field.

The evolution equation of the velocity field and the velocity equilibrium distribution function are shown in Equations 1 and 2 respectively.

$$f_\alpha(\boldsymbol{r}+\boldsymbol{e}_\alpha\delta_t, t+\delta_t) - f_\alpha(\boldsymbol{r},t) = -\frac{1}{\tau}\left[f_\alpha(\boldsymbol{r},t) - f_\alpha^{(eq)}(\boldsymbol{r},t)\right] + \delta_t F_\alpha(\boldsymbol{r},t) \quad (1)$$

$$f_\alpha^{(eq)} = \rho\omega_\alpha\left[1+\frac{e_\alpha \cdot \boldsymbol{u}}{c_s^2}+\frac{(e_\alpha \cdot \boldsymbol{u})^2}{2c_s^4}-\frac{u^2}{2c_s^2}\right] \quad (2)$$

The external force term can be expressed as:

$$F_\alpha = \left(1-\frac{1}{2\tau_f}\right)\omega_\alpha\left[\frac{\boldsymbol{e}_\alpha-\boldsymbol{u}}{c_s^2}+\frac{(\boldsymbol{e}_\alpha \cdot \boldsymbol{u})}{c_s^4}\boldsymbol{e}_\alpha\right] \cdot \boldsymbol{G} \quad (3)$$

$$\boldsymbol{G} = -\beta(T-T_0)\boldsymbol{g} \quad (4)$$

The temperature field evolution and the temperature equilibrium distribution function can be written as:

$$T_\alpha(\boldsymbol{r}+\boldsymbol{e}_\alpha\delta_t,t+\delta_t)-T_\alpha(\boldsymbol{r},t)= -\frac{1}{\tau_T}\left[T_\alpha(\boldsymbol{r},t)-T_\alpha^{(eq)}(\boldsymbol{r},t)\right] \quad (5)$$

$$T_\alpha^{(eq)}=\omega_\alpha T\left[1+\frac{\boldsymbol{e}_\alpha\cdot\boldsymbol{u}}{c_s^2}+\frac{(\boldsymbol{e}_\alpha\cdot\boldsymbol{u})^2}{2c_s^4}-\frac{u^2}{2c_s^2}\right] \quad (6)$$

Since the velocity field and temperature field are both D2Q9 models, their weight coefficients $\omega_\alpha$and lattice sound velocities have the same values, they are defined as:

$$e_\alpha = c\begin{bmatrix}1 & 0 & -1 & 0 & 1 & -1 & -1 & 1 & 0\\ 0 & 1 & 0 & -1 & 1 & 1 & -1 & -1 & 0\end{bmatrix} \quad (7)$$

$$c_s=\frac{c}{\sqrt{3}} \quad (8a)$$

$$\omega_\alpha=\begin{cases}\frac{4}{9}, c_\alpha^2=0\\ \frac{1}{9}, c_\alpha^2=c^2 \\ \frac{1}{36}, c_\alpha^2=2c^2\end{cases},\alpha=1\sim9 \quad (8b)$$

By Chapman-Enskog expansion of Eq. (1) and (5), the Navier-Stokes equations can be obtained, and it can be proved that the model has second-order accuracy. The macroscopic parameters of the whole flow heat transfer process are given by:

$$\rho=\sum_\alpha f_\alpha \quad (9a)$$

$$\rho u=\sum_\alpha f_\alpha e_\alpha \quad (9b)$$

$$p=\rho c_s^2 \quad (9c)$$

$$T=\sum_{\alpha=1}^{9}T_\alpha \quad (10a)$$

$$\nu=\frac{1}{3}c^2\left(\tau_f-\frac{1}{2}\right)\delta_t \quad (10b)$$

$$\chi=\frac{1}{3}c^2\left(\tau_T-\frac{1}{2}\right)\delta_t \quad (10c)$$

Since the model studied contains two different media, fluid and soil particles, the relaxation time in the temperature distribution function cannot be expressed by a unified value, but consists of the relaxation time of fluid and the relaxation time of soil solid particles, which is a matrix corresponding to the physical model. According to Wang et al., the above two types of relaxation time can be defined as:

$$\tau_{Tf}=\frac{3}{2}\frac{k_f}{(\rho c_p)_f c^2\delta_t}+\frac{1}{2} \quad (11a)$$

$$\tau_{Ts}=\frac{3}{2}\frac{k_s}{(\rho c_p)_s c^2\delta_t}+\frac{1}{2} \quad (11b)$$

(2) Verification of algorithm

The closed square cavity natural convection is a classic example of computational fluid dynamics and computational heat transfer. This problem involves the coupling of velocity field and temperature field, and the flow situation will change with the change of Rayleigh number. The overall situation is relatively complex, so it can be used to verify the correctness of the DDF-LBE model of incompressible flow and programming. The physical model of natural convection in closed square cavity is shown in Fig.1:

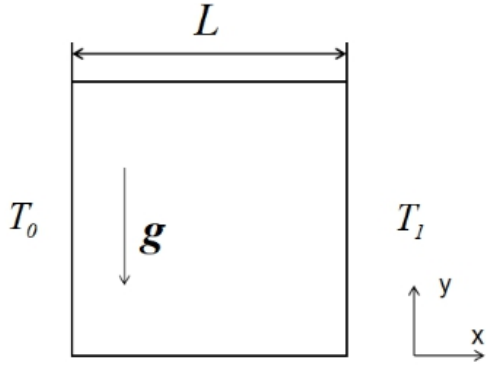

Fig.1 Physical model of closed square cavity natural convection

The temperature on the left wall of the square cavity is T_0, and the temperature on the right wall is T_1,$T_0 > T_1$. The temperature on the two walls is kept constant, and the upper and lower walls are insulated. The inside of the square cavity is filled with homogeneous and uniformly warm air, $P_r = 0.71$, which is only affected by gravity and is in the negative direction of the axis. The initial conditions and boundary conditions are taken to be:

Initial conditions: $u=0, T_m=\frac{T_0+T_1}{2}$ (12)

Boundary conditions:

$$u=0,\ T_{left}=T_0,\ T_{right}=T_1,\ \frac{\partial T}{\partial y}=0 \quad (13)$$

The natural convection in a closed square cavity with a lattice of 200×200 and $R_a = 10^3 \sim 10^6$ was simulated by programming, and the temperature distribution in the cavity under different conditions was obtained.

It can be seen from the Fig.2 that, with the increase of, the isotherms around the left and right boundary remain vertical, while the other isotherms change from vertical to horizontal direction. This phenomenon is consistent with the simulation of He Yaling[14].The reason for this phenomenon is that the heat transfer in the square cavity is mainly heat conduction when it is small. With the increase, the convective heat transfer gradually increases and finally dominates. At the same time, the flow field in the square cavity is constantly elliptical, which leads to the constant trend of the internal isotherm to the level.

Table1 Comparison of $Nu_{col,ave}$ in literature and simulation

Ra	Literature $Nu_{col,ave}$	This paper $Nu_{col,ave}$	Relative error/%
10^3	1.118	1.106	1.1
10^4	2.2448	2.2027	1.9
10^5	4.5216	4.5863	1.4
10^6	8.8251	8.8039	0.2

Table1 compares the average Nusselt number of the simulated cold wall surface with the literature [15-16] to further verify the correctness of the simulation. As can be seen from Table1, the relative errors between the simulation results and the literature results are all within 5%, which further proves the accuracy of the simulation.

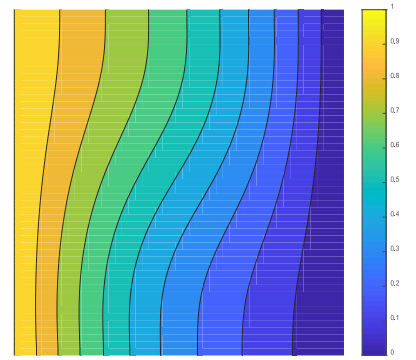

a) $Ra = 10^3$

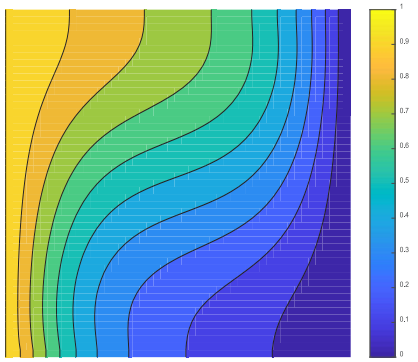

b) $Ra = 10^4$

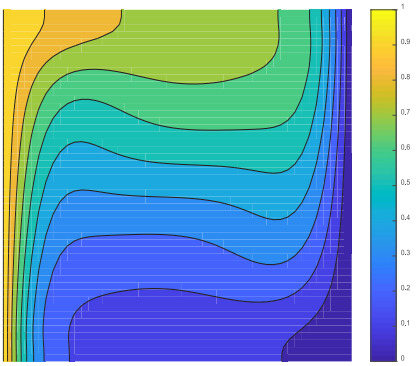

c) $Ra = 10^5$

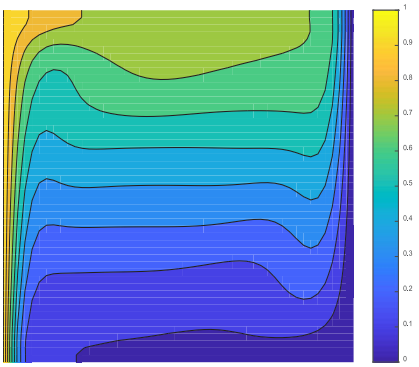

d) $Ra = 10^6$

Fig.2 Diagram of internal cavity isotherms under different Ra

3. PHYSICAL MODEL AND BOUNDARY CONDITIONS

(1) Physical model

According to the research of Li Jialin et al[17]., U-shaped buried pipes can be equivalent to equivalent diameter buried pipes for research, so as to simplify the model. At the same time, the temperature in the simulation process is expressed as the dimensionless excess temperature. The equivalent diameter and dimensionless excess temperature can be calculated as:

$$D_e = \sqrt{2D_o L_g} \tag{14}$$

$$T_r = \frac{T - T_{min}}{T_{max} - T_{min}} \tag{15}$$

Fig. 3 shows the simplified buried tube heat exchanger of equivalent diameter and its horizontal section diagram, this study will simulate the physical model shown in the figure and carry out in-depth research. The soil porous media generated by QSGS method is used inside the simulated area, and the groundwater flow in the soil only considers the flow from left to right in a single direction, that is, it enters from the left boundary at a speed, percolates to the right, flows through the buried pipe heat exchanger, carries on heat exchange with it, and finally flows out at a speed. During the simulation, the surrounding boundary of the simulation area and the buried pipe are kept constant temperature, $T_0$and T_1 respectively.

To simplify the physical and mathematical model, the following assumptions are made:

a) The soil is an isotropic porous medium, and the magnitude of macroscopic tensor does not change with direction;

b) The soil is a saturated porous medium, the pores are full of fluid and the fluid in the pores does not undergo phase transformation;

c) the deformation of soil pore structure during soil stratification and flow heat transfer is ignored;

d) Thermophysical parameters of soil will not change in the process of flow heat transfer;

e) satisfies the local thermal equilibrium hypothesis;

f) The buried pipe is a constant heat source.

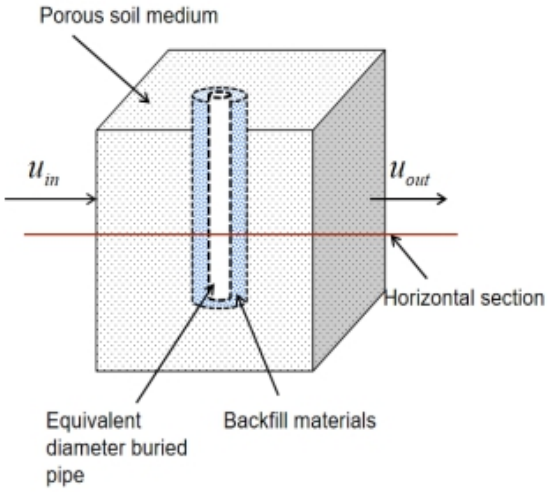

a) Diagram of equivalent diameter buried pipe

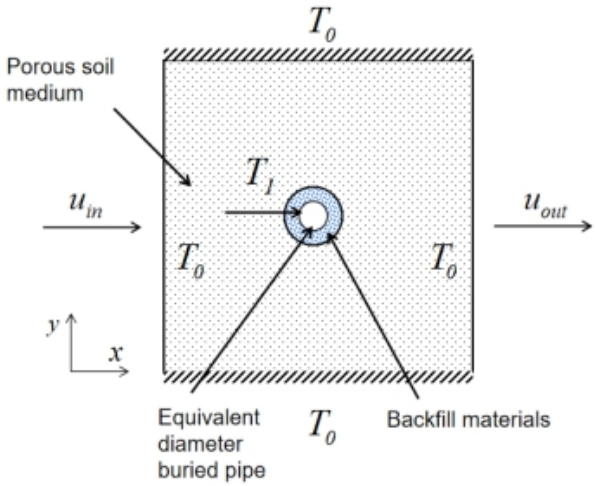

b) Diagram of section plane

Fig.3 Physical model diagram

(2) Initial conditions and boundary conditions

In numerical simulation, sets the initial temperature of the underground soil and fluid to 288.15 K, buried pipe temperature is 300.15 K, fluid density is 999.10 kg/m^3, the motion of fluid viscous coefficient of 1.141 × 10^{-6} m^2 / s, the specific heat at constant pressure fluid is 4.2 × 10^3 j/(kg · K), soil coefficient of thermal conductivity

of the solid skeleton is 1.5 W/(m K), the hole diameter is 150 mm, equivalent buried pipe diameter of 50 mm, for the coefficient of thermal conductivity of backfill materials, did not do so in the case, both to set the value equal to the coefficient of thermal conductivity of soil skeleton. Because the outer diameter of the buried pipe is only 50mm, the grid area of the 1m×1m simulation area is small and can be clearly expressed. If the simulation area is too large, the buried pipe is difficult to be clearly expressed in the model. Although the large grid number can improve the computational accuracy to some extent, the computational efficiency will be greatly reduced. According to the study of Tian et al[18], the 200×200 grid number can improve the computational efficiency on the premise of ensuring the computational accuracy. Therefore, the actual size of the simulated area is 1m×1m, and the corresponding grid number is 200×200. The time step and lattice step are both 1, and the lattice density is also 1. As mentioned above, in order not to violate the requirements of phase interface temperature and heat flow continuity, the volumetric heat capacities of different media can be made the same to solve the conjugated heat problem between different phases. In this study, the volumetric heat capacities of fluids are collected. The non-equilibrium extrapolation scheme is used to simulate the boundary of the model, and the standard rebound boundary scheme is used to simulate the boundary between the fluid and the soil particles and the heat exchange tube. In order to simplify the physical model, this paper only studies the heat transfer law between pore water in wet saturated soil and buried pipe heat exchanger. Therefore, without any explanation, the default porosity of the soil is 0.6, the growth and distribution probability of solid particles is 0.01, and the fluid in the pores is water.

4.SIMULATION RESULTS AND ANALYSIS

(1) Effect of porosity on heat transfer in buried pipes

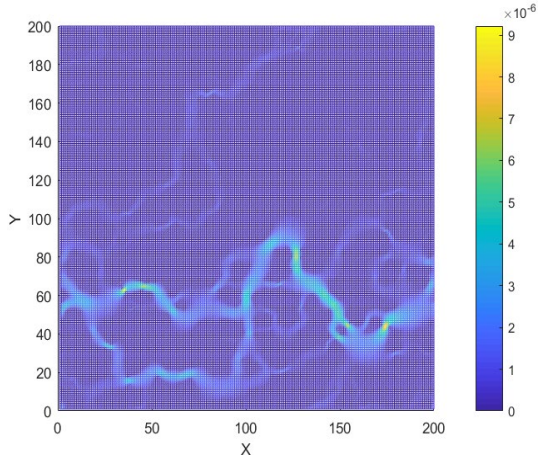

a) $\varepsilon = 0.6$

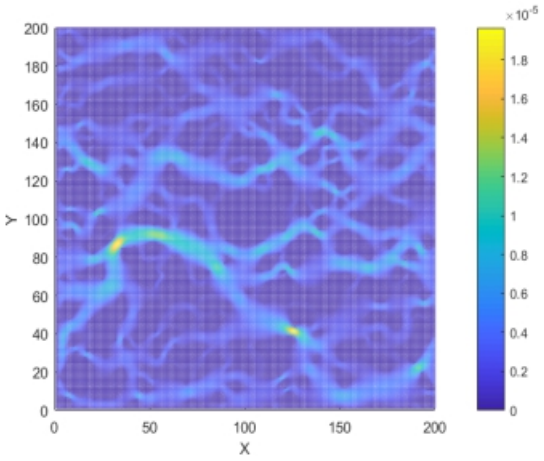

b) $\varepsilon = 0.8$

Fig.4 Velocity distribution in soil with different porosity

Fig. 4 shows the velocity distribution diagram of the seepage in the soil with porosity of 0.6 and 0.8. It can be seen from the figure that the number of pore channels has increased a lot and the width of channels has also increased. With the increase of porosity, the number and width of pore channels also increase the flow velocity of pore water. When the porosity is 0.6, the average flow velocity is 2.8753×10^{-7}, while when the porosity is 0.8, the average flow velocity is 9.92×10^{-6}. Therefore, the

flow velocity of pore water increases a lot relatively.

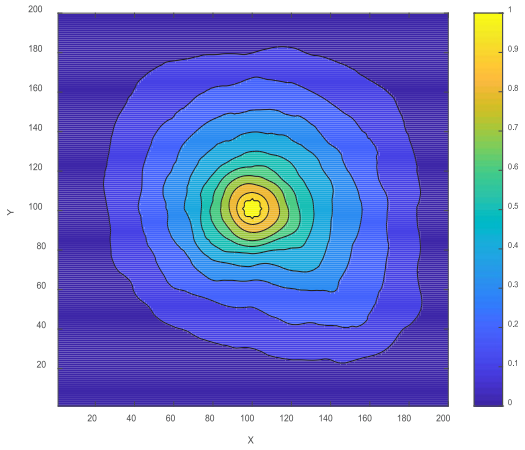

a) $\varepsilon = 0.6$

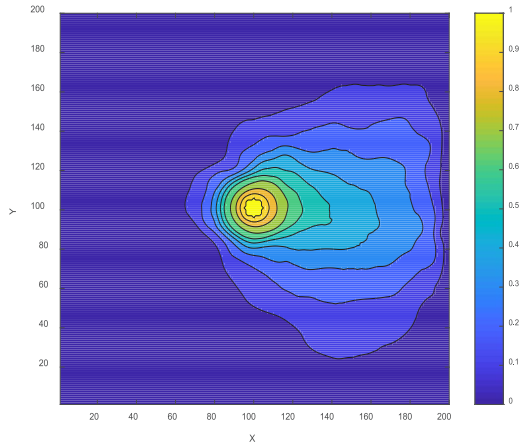

b) $\varepsilon = 0.8$

Fig.5 Cloud image of temperature distribution at different porosity

Fig. 5 shows the temperature distribution in the simulated area when the porosity is 0.6 and 0.8. It can be seen from the figure that when the porosity is 0.6, the temperature distribution is approximately circular, and the isotherm spacing at the seepage passage on the right side of the buried pipe increases, and the temperature change slows down. When the porosity is 0.8, the temperature distribution is approximately fan-shaped, and the buried pipe only has heat exchange with the soil in a small range on the left side, while there is an obvious temperature distribution on the right side of the buried pipe, and the distance between isotherms and isotherms is large. Appear this kind of phenomenon the reason is that with the increase of porosity, pore channel number increasing, the seepage velocity of pore water, pore water proportion increase, more pore water with relatively greater seepage velocity and convective heat transfer of buried pipe, and the pore water is along the flow direction will be away from heat, cause inverse seepage flow in the direction of heat transfer.

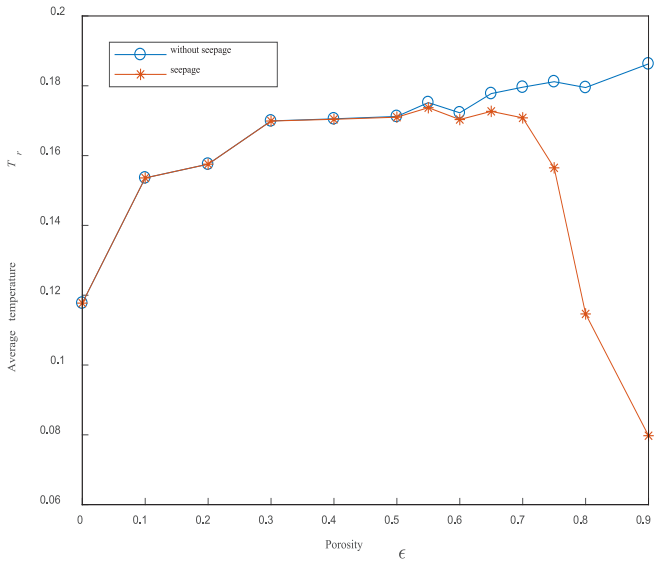

Fig.6 The relationship between regional average temperature and porosity is simulated

Fig. 6 shows the relationship curve between the average temperature and porosity in the simulated area with and without seepage. As can be seen from the figure, with the increase of porosity, the average temperature in the simulated area without seepage keeps rising. When there is seepage flow, the average temperature first rises and then stays basically unchanged, and finally decreases. By comparing the two cases of temperature curve can also discover that in the range of porosity of 0 ~ 0.5, the average temperature of the inside of the seepage on soil size have little impact, when the porosity is higher than 0.5, the average temperature of the soil without seepage is relatively higher, with increasing of the temperature difference between seepage. Average temperature appear this kind of change is because in 0 ~ 0.5 the scope of low porosity, soil internal little throughout the entire simulation area around the

border of the seepage channels or pores little and narrow, cause pore water seepage rate is extremely low, no seepage velocity or the heat exchange between soil and ground heat exchanger is still predominantly thermal conductivity. With the increase of porosity, the proportion of pore water increases, and because the thermal conductivity of water is lower than that of soil solid particles, the average temperature in the region is gradually rising regardless of the existence of seepage, and the change of average temperature is basically the same. When the porosity is higher than 0.5, both the number and width of seepage channels in the soil increase with the increase of porosity. At this time, the seepage velocity keeps increasing and the influence of seepage is also gradually increasing, which can be roughly divided into two parts. The first part is that when the porosity is between 0.5 and 0.7, the pore channels inside the soil gradually increase, the width of the channels increases, and the seepage velocity also increases. At this time, the influence of seepage on heat transfer gradually increases. When the direction of seepage is consistent with the direction of heat conduction, convective heat transfer strengthens the heat transfer between soil and buried pipe, and the isotherm moves backward. When the direction of seepage is opposite to the direction of heat conduction, the fluid flow takes away the heat on the side, and the convective heat transfer weakens the heat transfer between the buried pipe and the soil. In this range, due to the limited seepage channels and the increase in the proportion of water in the soil, the average temperature in the region with seepage is basically kept at the same level, but it does not exist in the absence of seepage. As the temperature gradually increases, the temperature difference between the two starts to appear and keeps increases. The second part is when the porosity is higher than 0.7, the amount of seepage channel greatly increased and the mutual connection, the seepage velocity is increasing, the soil solid phase proportion constantly decreases, and the heat transfer between the buried pipe and soil with convective heat transfer is given priority to, seepage heat-exchange strengthening and weakening the role of more obvious, the average temperature of the simulation area and therefore reduce rapidly, while without seepage, the average temperature of the soil is still in a slight amplitude, temperature difference between the two greatly increased.

(2) Effect of seepage velocity on heat transfer

Fig. 7 is the temperature distribution nephogram of the simulated area under different seepage velocities. It can be seen from the figure that, when the seepage velocity is 0, that is, when there is no seepage, the isotherm is approximately elliptical, the tortuous degree of the isotherm is also low, and the overall distribution is relatively uniform. This is because when using matrix to construct the physical model, the buried pipe is approximately round due to the restriction of integer grid points, so the isotherms in the temperature cloud map are approximately elliptical. Moreover, due to the different thermal conductivity between the soil skeleton and pore water, all the isotherms are tortuous to varying degrees. With the increase of infiltration speed, the uniformity of temperature distribution is getting worse, the influence range of buried pipe on the left side is also shrinking, and the isotherm spacing is shrinking. On the lower right side, on the contrary, the influence range of buried pipe is constantly expanding, and the isotherm spacing is constantly increasing in this direction. This is because with the increase of seepage velocity, seepage has more and more influence on the heat transfer of buried pipe. When the direction of heat transfer is opposite to the direction of seepage, the heat transfer is more difficult, and the influence range of buried pipe is decreasing. When the direction of heat transfer is consistent with the direction of seepage, the heat transfer is strengthened, the isotherm protrudes outward along the seepage channel, and the influence range of buried pipes expands along the direction of the seepage channel.

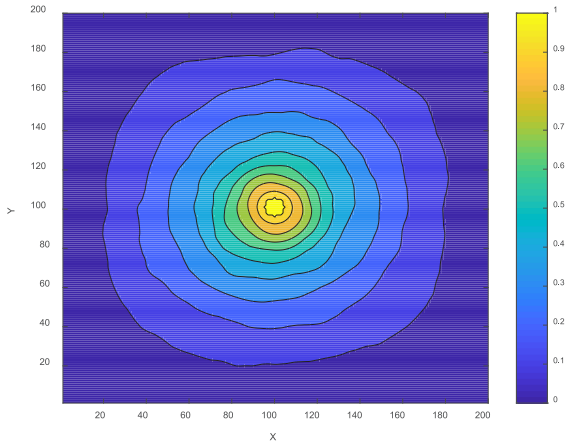

a) $u_0 = 0$ m/s

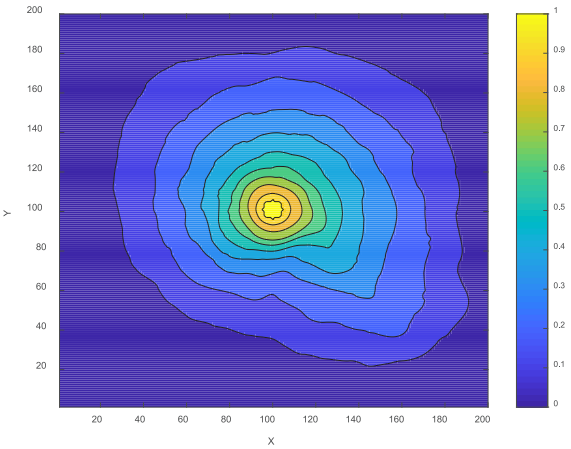

b) $u_0 = 1.5 \times 10^{-5}$ m/s

Fig.7 Temperature cloud map under different seepage velocities

Fig. 8 shows the relationship curve between the average temperature in the simulated area and the initial velocity of seepage. It can be seen from the figure that when the velocity of seepage is less than or equal to 2×10^{-6}m/s, the average temperature in the simulated area almost does not change. This is because the seepage velocity is small, so the heat exchange is given priority to with thermal conductivity, convective heat transfer caused by pore water flow on almost can ignore the influence of buried tube heat exchanger, with seepage velocity increasing, the seepage direction inverse heat transfer has been weakened and heat taken away by pore water, only in the seepage direction near space channel heat transfer is significantly enhanced, so the temperature of the whole simulation area showed a trend of decline, falling speed is accelerating.

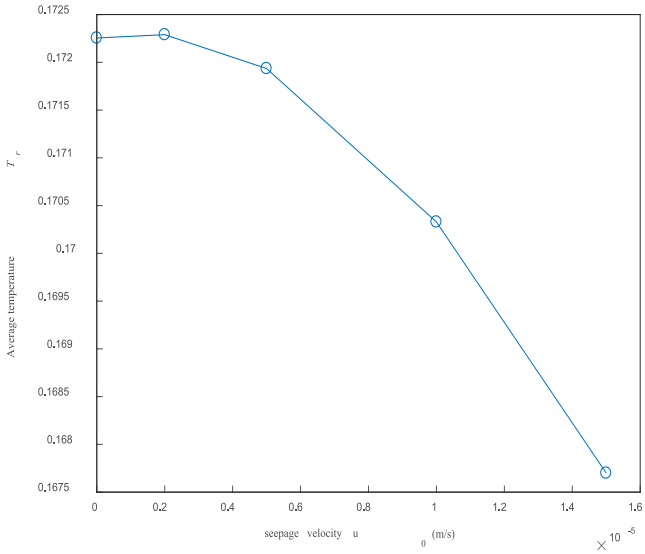

Fig.8 Relationship curve between average temperature and initial infiltration velocity

(3) Effect of soil particle distribution on heat transfer

Fig. 9 shows the velocity distribution in the simulated area when p_0 is 0.05 and 0.01. As can be seen from the above, when p_0 is 0.05, soil particles are small, the distribution is uniform, and the pore connectivity is high. Therefore, as shown in Figure a), most pore water is in a state of flow with a certain seepage velocity, and the velocity distribution in the simulated area is relatively uniform. When p_0 is 0.01, the degree of soil particle aggregation is high, and part of the pores are surrounded by solid phase so that the internal fluid cannot flow. Therefore, the whole simulated area only has the corresponding velocity at the seepage channel, and the rest of the seepage velocity is very small or no.

By comparison, under the condition of the same infiltration velocity, although the velocity distribution is relatively uniform when p_0 is 0.05, the overall velocity size is lower than that when p_0 is 0.01. In Fig. a), the seepage velocity of pore water is mostly below 1×10^{-6}m/s, while in Fig. b), the seepage velocity of pore water is mostly between 1×10^{-6}m/s ~ 4×10^{-6}m/s with velocity. Meanwhile, the maximum seepage velocity in Fig.

b) is also higher than that in Fig. a). This phenomenon occurs because the particle distribution is uniform when p_0 is large, although most of the pore water can flow, but the pore size is too small, no obvious seepage channel simulation area, in the process of the flow resistance is relatively large, the overall seepage velocity at lower levels, and p_0 smaller cases, simulation of obvious seepage channel and channel in the area of relatively large size, so that the flow of the pore water in the channel rate relatively larger.

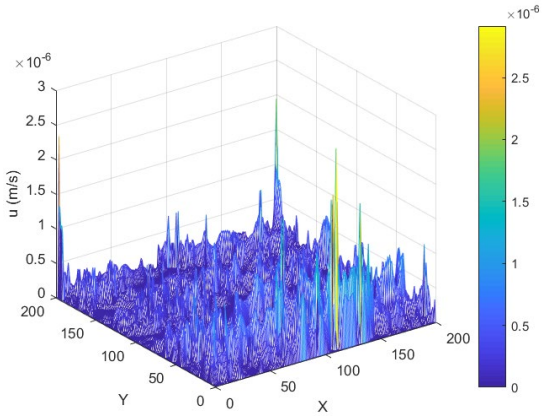

a) $\varepsilon = 0.6,\ p_0 = 0.05$

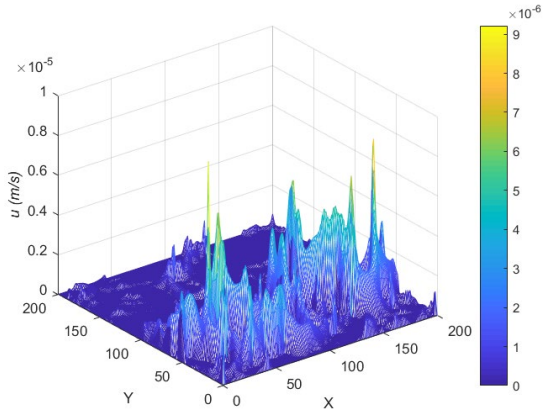

b) $\varepsilon = 0.6,\ p_0 = 0.01$

Fig.9 Seepage velocity distribution diagram of simulated region under different $p_0$conditions

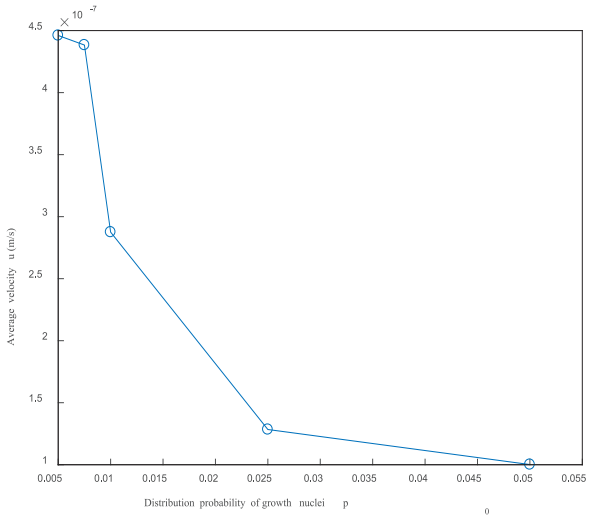

Fig.10 Relation curve between average velocity and p_0 in the simulated area

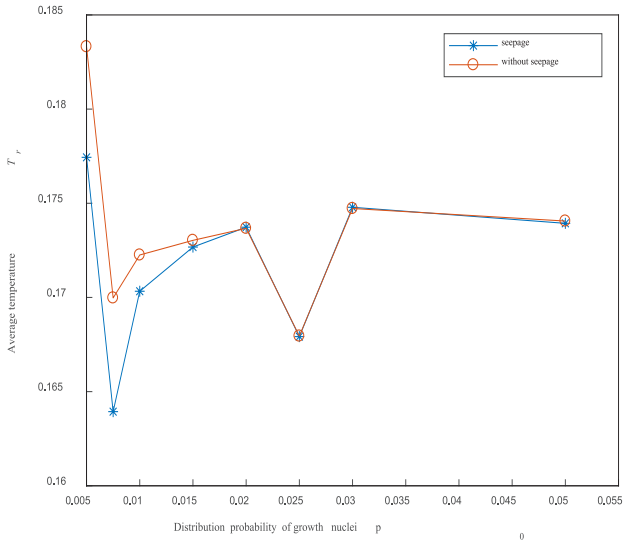

Fig. 11 The relationship between the mean temperature and p_0 in the simulated area

Fig. 10 for simulation area under the same initial infiltration rate, the relationship between average speed and curve can be found from the figure, with the increase of p_0, the average flow velocity and decreases, this is because the large pore connectivity, there are many branches around the seepage channels, when $p_0$is small, pore water is often only along the flow of the seepage passage.

Fig. 11 is the relationship curve between the average temperature in the simulated area and p_0. It can be seen from the figure that, with or without seepage flow, with the increase of, the average temperature in the simulated area does not change

monotonously, but presents an irregular change alternatively between decreasing and rising. There are two reasons for this phenomenon. The first reason is that the size of p_0 determines the distribution and accumulation degree of soil solid particles in the simulated area, and has a significant impact on the number and pattern of pore channels in the soil, thus affecting the heat transfer and temperature distribution within the whole area. Secondly, due to the randomness of the generation of porous media models, even if the initial conditions are exactly the same, the generated models also have certain differences. It is the differences between the models that make the average temperature in the simulated area fluctuate to a certain extent.

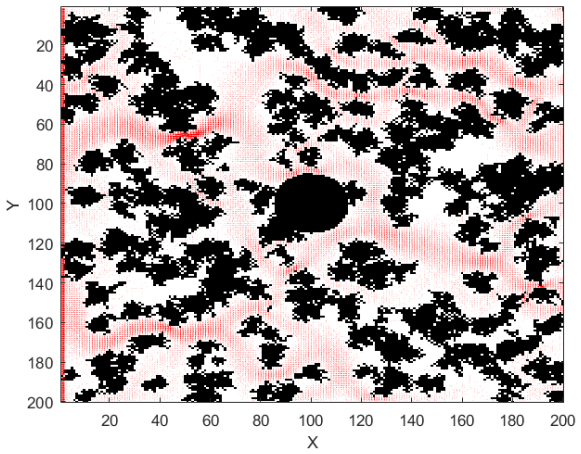

a) The porous media model 1

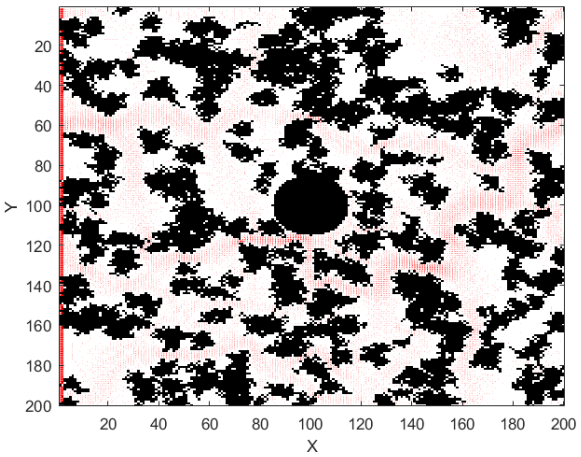

b) The porous media model 2

Fig.12 Porous media models of $\boldsymbol{\varepsilon = 0.6, p_0 = 0.0075}$

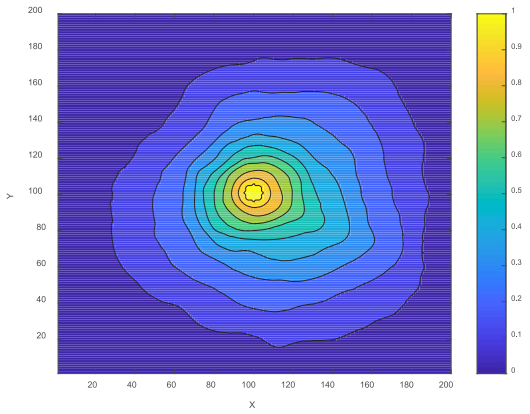

a) Temperature distribution nephogram of porous media model 1

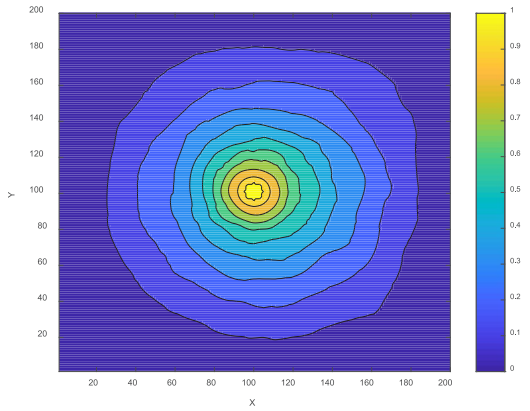

b) Temperature distribution nephogram of porous media model 2

Fig.13 Temperature distribution nephogram of $\boldsymbol{\varepsilon = 0.6, p_0 = 0.0075}$

It can also be found, when p_0 is greater than or equal to 0.02, with an average temperature and seepage under the condition of simulation area without seepage are basically equal, this is because the soil particles are evenly distributed, has seepage channel width is small, the seepage velocity is very small, thermal simulation area dominated, convective heat transfer is almost negligible. Therefore, the average temperature in the simulated area is basically the same in both cases.

Fig. 12 and Fig. 13 shows two different models of porous media generated in this case and their temperature distribution cloud maps. It can be seen from the figure that, even if the initial conditions are exactly the same, the generated models have certain differences and the temperature distributions are also different. After calculation, a) the average

temperature of the simulated area in Model 1 shown in Figure 13 is 0.1639; b) the average temperature of the simulated area in Model 2 shown in Figure 13 is 0.1713. This is because when p_0 is small, the degree of soil particle aggregation is high, and the generated model has a certain probability that there is no effective pore channel, which makes the overall temperature of the simulated region high. Once an effective pore channel is formed, the width of the channel is relatively large, the flow rate of pore water is also large, and part of the heat is taken away, so that the overall temperature is low.

(4) Effect of thermal conductivity of soil skeleton on heat transfer

Fig. 14 shows the temperature distribution cloud map in the simulated area under different k_s. With the increase of k_s, the tortuous degree of each isotherm increases continuously, and the influence range of buried pipes also increases to some extent. Meanwhile, through comparison, it can be clearly seen that the isotherm change caused by seepage is almost invisible in figure b).Appear this kind of phenomenon is because, with the increase of k_s , the solid particles are more conducive to heat conduction, and the gap between water coefficient of thermal conductivity of solid phased particles increases the difference, along the direction of heat flow on both ends of the temperature difference of solid phased particles decreases, and the whole simulation area of heat conduction is continuously strengthen, seepage channel near the inverse heat transfer weaken the effect of seepage direction have been offset, and isotherm, decrease of smooth degree of the influence of the buried pipe range increases to A certain extent, caused by seepage isotherm seepage channel along the direction of change are covered.

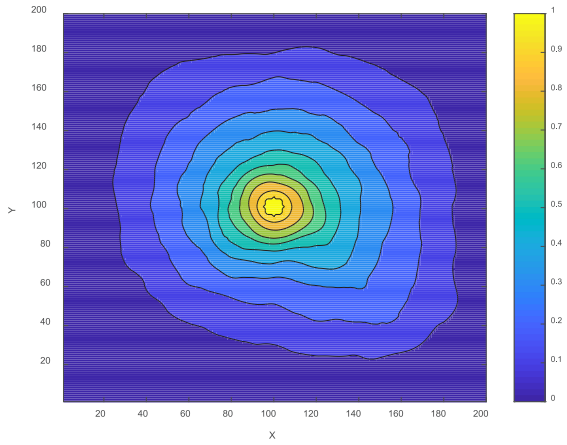

a) $\varepsilon = 0.6,\ k_s = 1.5$

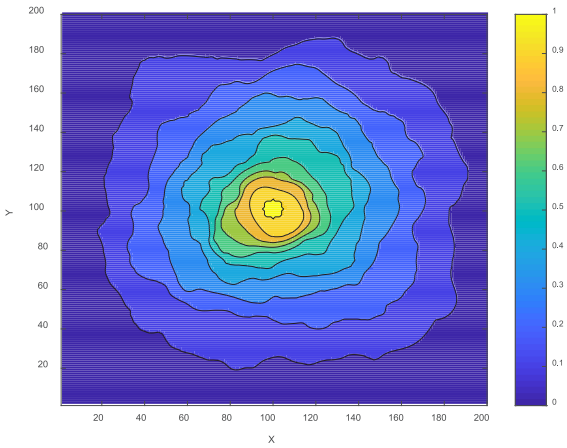

b) $\varepsilon = 0.6,\ k_s = 5.5$

Fig.14 Temperature nephogram in the simulated region at different k_s

Fig. 15 shows the relationship curve between the average temperature in the simulated area without and with seepage. It can be seen from the figure that, with the increase of k_s, the average temperature in the region is increasing in both cases, but it does not increase linearly. The growth trend of the average temperature in both cases is similar. At the same time, it can be found that when k_s is small, and the average temperature without seepage is higher than that with seepage. With the increase of k_s, the temperature difference between them decreases continuously. When k_s is 5.5W/ (m·K), the average temperature is basically the same. That's because at a certain seepage velocity, solid phase between solid phase and solid phase before between pore water and heat, heat is taken away by flow of pore water, the existence of seepage weakened the overall heat transfer, k_s seepage

heat-exchange has great influence, is small, with the increase of k_s thermal conductivity occupied the main position, and the influence of seepage almost negligible. In the case of seepage, the average soil temperature is relatively low. When the temperature is higher than 5.5W/ (m·K), the influence of seepage on the heat transfer of buried pipes is almost negligible, and the average temperature in the soil is basically the same.

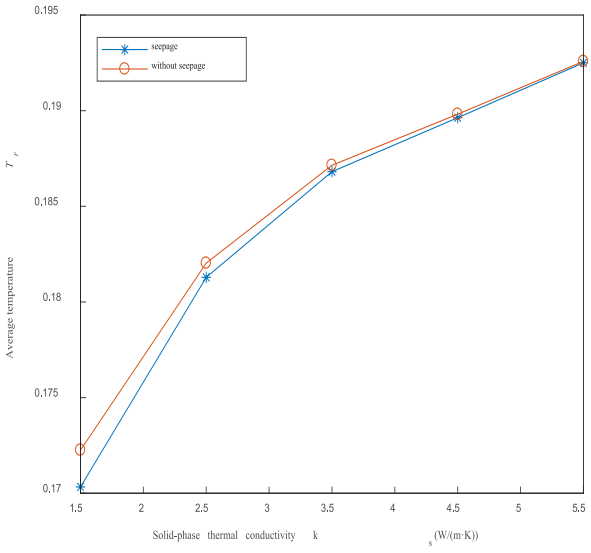

Fig.15 Relation curve between average temperature and k_s

5.CONCLUSIONS

In this paper, QSGS method was used to construct the soil porous medium model. Through the incompressible DDF-LBM model based on Boussinesq hypothesis, the influences of four factors, such as porosity, seepage velocity, soil particle distribution and soil skeleton thermal conductivity, on the heat transfer between the buried pipe heat exchanger and soil were studied, and the following conclusions were drawn.

a) When other conditions are the same, the average soil temperature without seepage increases with the increase of porosity. When seepage is present, the average soil temperature first increases, then basically stays unchanged, and finally decreases rapidly. When the porosity is lower than 0.5, the average temperatures of soil with and without seepage basically coincide with each other, and then the temperature difference between them gradually becomes larger.

b) When other conditions are the same, the seepage velocity at the outlet of the model increases linearly with the increase of the initial infiltration velocity, and the soil temperature basically does not change when the seepage velocity is less than or equal to 2×10^{-6}m/s, and then decreases with the increase of the seepage velocity, and the decreasing rate gradually accelerates.

c) Other conditions being the same, with the increase of p_0, the seepage velocity in the simulated area decreases continuously. With or without the presence of seepage, the average temperature of the soil then presents an irregular change alternately of rising and falling. When p_0 is less than or equal to 0.02, the average temperature of the soil without seepage is higher than that with seepage, and then the two temperatures almost coincide with each other.

d) Other conditions being the same, the tortuous degree of soil isotherm increases with the increase of k_s, and the average soil temperature increases with or without seepage. When k_s is higher than 5.5W/ (m·K), the effect of seepage can be basically ignored, and the two average soil temperatures become to coincide with each other.

APPENDIX

Nomenclature

c	Lattice velocity
c_s	sound speed,$c_s^2 = 1/3$
D_e	Equivalent tube outside diameter
D_o	U-tube outside diameter
e_α	The velocity space of finite dimension is simplified by the velocity
f_α	velocity distribution function
$f_\alpha^{(eq)}$	Equilibrium velocity distribution function
$\boldsymbol{F_\alpha}$	External force
$\boldsymbol{g}$	Acceleration due to gravity,$(m \cdot s^2)$
$\boldsymbol{G}$	Effective external force

h	Convective heat transfer coefficient, $(W/(m^2 \cdot K))$
k_i	The corresponding thermal conductivity of each medium
L_g	Tube pitch
Nu	Nusselt number
p	Pressure
p_0	Distribution probability of growth nuclei
Pr	Prandtl number,$Pr = \nu/\chi$
$\boldsymbol{r}$	a lattice point in a lattice region
Ra	Rayleigh number,$Ra = \boldsymbol{g}\beta\Delta T L^3/\nu^3$
Re	Reynolds number,$Re = u_0 D/\nu$
t	time
T_0	Initial temperature, (K)
T_α	Temperature distribution function
$T_\alpha^{(eq)}$	Equilibrium temperature distribution function
ΔT	Temperature difference, (K)
$\boldsymbol{u}$	velocity
β	Coefficient of thermal expansion
δ_t	time step
ν	Kinematic viscosity, (m^2/s)
ρ	Density, (kg/m^3)
$(\rho c_p)_i$	The corresponding volume heat capacity of each medium
χ	Thermal diffusivity coefficient, $(m^2 \cdot S)$
ε	porosity
τ_f	Relaxation time of f_α
τ_T	Relaxation time of T_α
w_α	Weight coefficient

REFERENCES

1) Liu W, Zhang Z Q, Liu W M, et al.: Effects of Groundwater Seepage on Soil Temperature Field Around Vertical U-Shaped Buried, *J. Journal of Building Energy Efficiency.,* Vol.48, Pt.353, pp.21-26,2020.
2) Wang Y, Liu Z C.: Influence of Groundwater Seepage to the Heat Transfer Characteristics of Double U-type Ground Heat Exchanger Group in Heat Pump System，*J. Research and Exploration in Laboratory*., Vol.38, Pt.9, pp.52-57,2019.
3) Guo C M, Du Q Q, Ma J C, et al.: Research on the influence of ground heat exchanger partition operating on soil heat accumulation, *J. Journal of Thermal Science and Technology*., Vol.17, Pt.4, pp.259-266,2018.
4) Chiasson A D, Ress S J, Spitler J D.: A preliminary of the effects of ground-water flow on closed-loop ground-source heat pumps systems, *J. ASHRAE Trans*., Vol.106, pp.380-393,2000.
5) GEHLIN S E A, HELLSTR M G.: Influence on thermal response test by groundwater flow in vertical fractures in hard rock, *J. Renew able Energy*., Vol.28, Pt.14, pp.2221-2238,2003.
6) WANG M，PAN N.: Numerical analyses of effective dielectric constant of multiphase microporous media, *J. Journal of Applied Physics*., Vol.101, Pt.11, pp.114102-1-114102-8,2007.
7) Zhu W W, Yao Y D, Zou W, et al.: Pore Model Based on Quartet Structure Generation Set and Its Fractal Description, *J. Natural Gas and Oil.*, Vol.34, Pt.3, pp.64-68,2016.
8) Zhang J R, Zhong S W.: Fractal behaviors of microscope pore structure of soil reconstructed by quartet structure generation set, *J. Journal of Hydraulic Engineering*., Vol.49, Pt.7, pp.814-822,2018.
9) Tian Z W, Chen L.: Study on pore fracture structure and its size based on quartet structure generation set method, *J. Inner Mongolia Coal Economy*., Pt.11, pp.110-112,2017.
10) Shao B L, Wang S Y, Tian R C, et al.: 3D Lattice Boltzmann Simulation of Fluid Seepage in Porous Media, *J. Journal of Chemical Engineering of Chinese Universities*., Vol.32, Pt.5, pp.1073-1081,2018.
11) Gao D Y，Chen Z Q，Chen L H，et al.: A modified lattice Boltzmann model for conjugate heat transfer in porous media, *J. International Journal of Heat and Mass Transfer*., Vol.105, pp.673-683,2017.
12) Xu F, Zhang Y N, Liang S, et al.: Model development for infiltration of unfrozen water in saturated frozen soil using lattice Boltzmann method, *J. International Journal of Heat and Mass Transfer*., Vol.141, pp.748-756,2019.
13) Guo Z, Shi B, Zheng C.: A coupled lattice BGK model for the Boussinesq equations, *J. International Journal for Numerical Methods in Fluids*., Vol.39, pp.325-342,2002.
14) He Y L, Wang Y, Li Q.: Lattice Boltzmann Method: Theory and Applications, *M. Beijing: Science Press*, pp.31-32,2009.
15) Khanafer K, Vafai K, Lightstone M.: Buoyancy-driven heat transfer enhancement in a two-dimensional

enclosure utilizing nanofluids, *J. International Journal of Heat and Mass Transfer*., Vol.46, Pt.19, pp.3639-3653,2003.

16) Hortmann M, Peric M, Scheuerer G.: Finite volume multigrid prediction of laminar natural convection: Benchmark solutions, *J. International Journal for Numer Methods in Fluids*., Vol.11, pp.189-207,1990.

17) Li J L, Xu L.: Comparison and analysis of Heat Transfer Model between U Type Buried Pipe and Equivalent Diameter Buried Pipe, *J. Contamination Control and Airconditioning Technology CC&AC*, Pt.4, pp.24-28,2018.

18) Tian W，Liu Z C, Liu W.: Lattice Boltzmann Simulation of Flow and Heat Transfer in Porous Media, J. Advances in Energy and Power Engineering., Vol.7, Pt.2, pp.23-31,2019.